Chapter-6: Effect of Electrode Paste on O_2 Ions…..

6.1 Introduction

In electrolytes, control of ionic to electronic conductivity is very crucial to achieve high ionic conductivity. The oxide materials can be tuned as high oxide ion conductor for the electrolyte. The ratio of ionic conductivity to electronic conductivity was measured by transport number (T_f). On the basis of the value of this number, there are three types of electrical behaviour viz. Type I (oxide ion conductor, $t_{ion} \geq 0.85$), Type II (mixed ionic-electronic conductor $0.85 > t_{ion} > 0.10$) and Type III (electronic conductor $t_{ion} \leq 0.10$) [9]. In oxide ion solid electrolytes, high oxide ion conduction can be obtained by creating oxide ion vacancies into fluorite or perovskite type oxides by doping [104]. Out of the various perovskite oxide electrolyte materials, Lanthanum aluminate (LAO) shows high ionic conductivity, high chemical and mechanical stability also, which makes it suitable for electrolyte for SOFCs over other electrolytes. In the previous chapters, it is already mentioned that how an alio-valent substitution having larger ionic radii [19] (chapter 4) and an iso-valent substitution having smaller ionic radii (chapter 5) can affect the ionic conduction of LAO.

In the present chapter, the effect on the conduction mechanism of LAO using electrodes like Ag and Pt on the basis of the differential impedance data analysis by preparing two symmetrical cells Ag/M/Ag and Pt/M/Pt where M = $(La_{0.9-x}(A)_x)Sr_{0.1}Al_{0.9}Mg_{0.1}O_{3-\delta}$ (A = Ba, Sm) has been explained. Also, through differential impedance analysis, pathways for the electrode/electrolyte interface and reaction mechanism of symmetrical cells have been proposed.

6.2 Experimental

All the compositions $La_{0.9}Sr_{0.1}Al_{0.9}Mg_{0.1}O_{3-d}$ (B0, x = 0.00), $(La_{0.9-x}Ba_x)Sr_{0.1}Al_{0.9}Mg_{0.1}O_{3-d}$ (B3, x = 0.03) and $(La_{0.9-x}Sm_x)Sr_{0.1}Al_{0.9}Mg_{0.1}O_{3-d}$ (S3, x = 0.03) were prepared by auto combustion synthesis. Details of the experimental procedures were already reported in chapter 2. Silver (Ag) and platinum (Pt) paste were used as electrode on both faces of the sintered pellets and fired for 20 minutes at 700 °C and 900 °C, respectively. In order to understand the mixing of dopants in $LaAlO_3$, the crystal structure of the doped $LaAlO_3$ sample was analyzed using X-ray Diffractometer (XRD). The surface morphology was studied by using scanning electron microscopy (SEM) equipped with an X-ray energy dispersive spectrometer (EDS). The electrical conductivity of prepared sintered pellet was measured by employing two-probe impedance spectroscopy LCR meter (WK 6500P) in the temperature range 100°C-600 °C.

6.3 Results and Discussions

6.3.1 Phase Identification Using XRD

Base material LAO and $(La_{0.9-x}A_x)Sr_{0.1}Al_{0.9}Mg_{0.1}O_{3-\delta}$ (A= Ba, Sm for x = 0.0, 0.01 and 0.03), (abbreviated as B0, B1 and B3 for Ba substituted samples having doping concentration x = 0.0, 0.01 and 0.03, respectively. Similarly S1 and S3 for Sm substituted samples having doping concentration x = 0.01 and 0.03, respectively) were synthesized. The single-phase formation was observed for all these samples. Out of these six compositions only three compositions B0, B3 and S3 were chosen for the present investigation, i.e., $La_{0.9-x}(Ba/Sm)_xSr_{0.1}Al_{0.9}Mg_{0.1}O_{3-\delta}$ (x = 0.0, 0.03) were selected as representative samples. Fig.6.1 shows the XRD patterns of these samples, which is well matched with the base material LAO structure. All the diffraction peaks of sintered

specimens are identified as the single phase of a rhombohedral perovskite structure with space group R-3c using JCPDS file No. 82-0478.

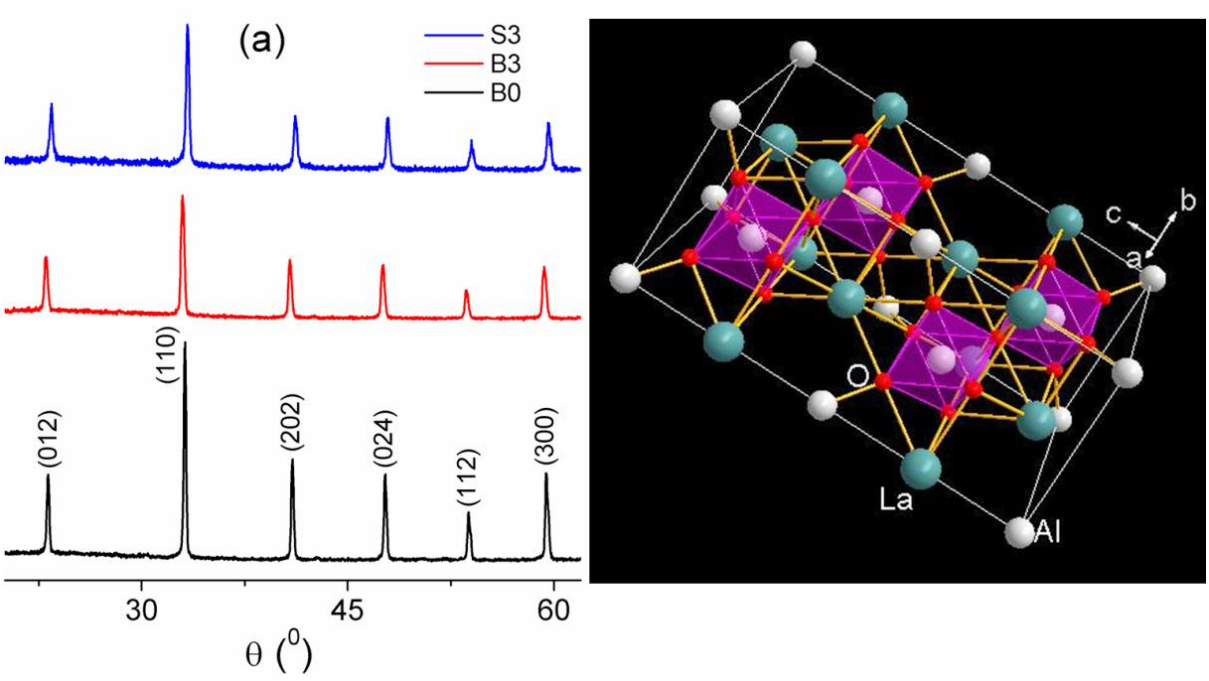

Figure 6.1: X-ray diffractograms of the samples B0, B3 and S3

6.3.2 Conduction at Electrode/Electrolyte Interface

In order to study the conduction behaviour comprehensively, it was prepared two symmetric cells Ag/M/Ag and Pt/M/Pt. It is well known that there are separate effects of Ag and Pt for the cathode reduction and the anode oxidation activity, i.e., Ag reacts faster than Pt for cathode reduction and Pt reacts faster than Ag in case of anode oxidation. Silver (Ag) easily makes oxide when reacts with metal oxide. A higher oxygen affinity means that the metal can take more oxygen from the gas phase or other source. Hence its oxidation rate will be higher, the metal will be oxidized to its oxide and its metallic activity will be lost and the trend for metallic activity will be Ag < Pt. Therefore, higher oxygen affinity leads to higher activity of oxygen and the rate-determining step will be the oxygen transport into the lattice of the materials [105]. In this way, Pt shows blocking

effect for oxide ions, especially in the temperature range 400-600 °C. Therefore, a study of both the cells should reveal a better insight picture.

6.3.3 AC Conductivity Analysis

In order to show the electroding effect on conductivity, it was studied the conductivity spectra for B0, B3 and S3 specimens for the both cell configurations and plotted log σ vs log ν as shown in Fig. 6.2 (a-f). The ac conductivity data, obtained for all these samples, were well fitted with the Jonscher power law in Eq. 2.4. It was observed that the conductivity was frequency independent at low frequencies and increased after a certain value with the increasing frequency. However, at high frequency, the conductivity spectra exhibit dispersion, increasing in the form of power-law and tend to form another plateau in low temperature regime and then this plateau becomes invisible in the high temperature regime. Also, using Jonscher Power law fitting, dc conductivity (σ_{dc}), exponent (n) and hopping frequency (ν_h) were calculated.

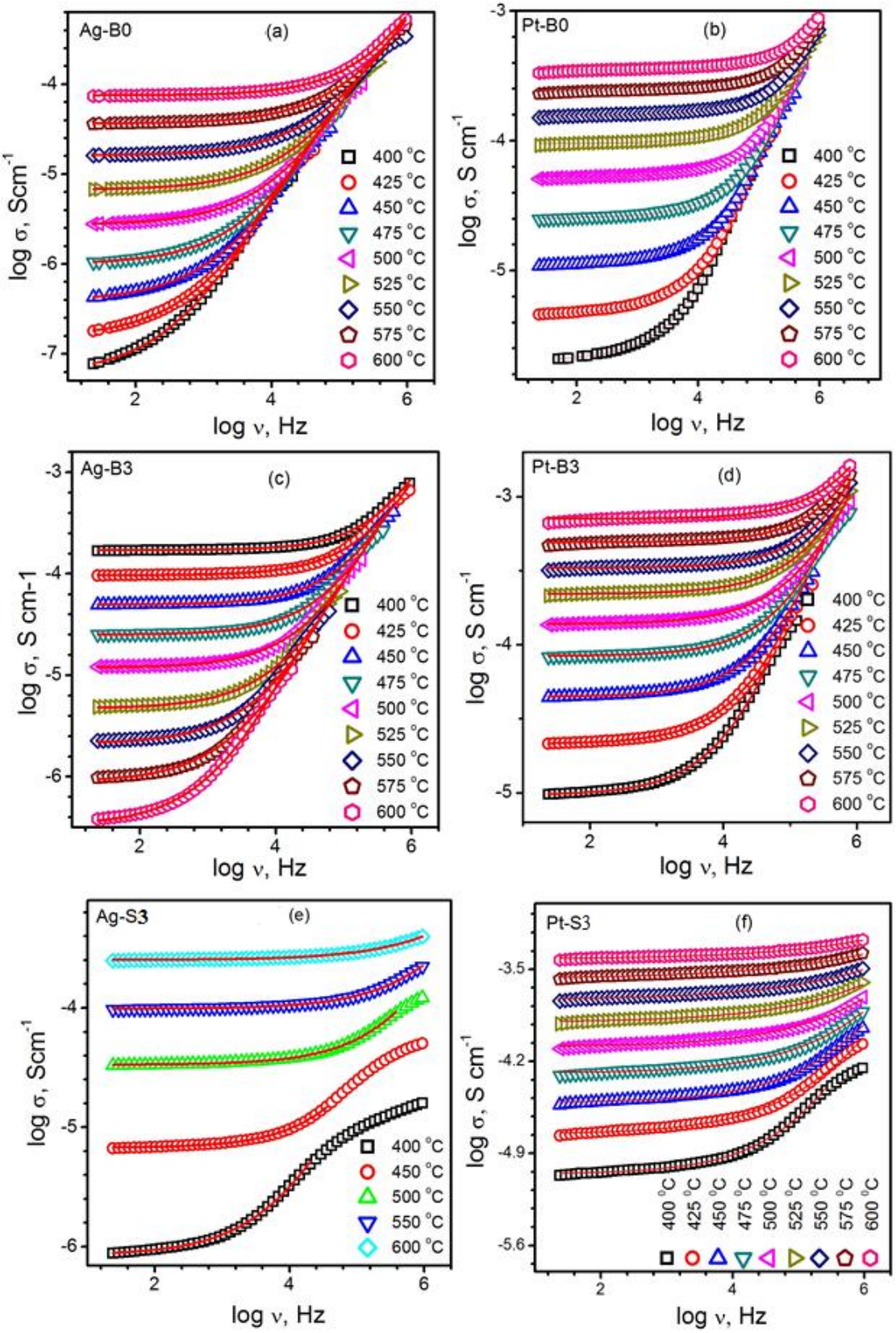

Figure 6.2: (a-f) shows log σ vs log ν for B0, B3 and S3 specimens with both cell configurations. The symbols indicate the data points and lines represent the fitting to the data through J P law

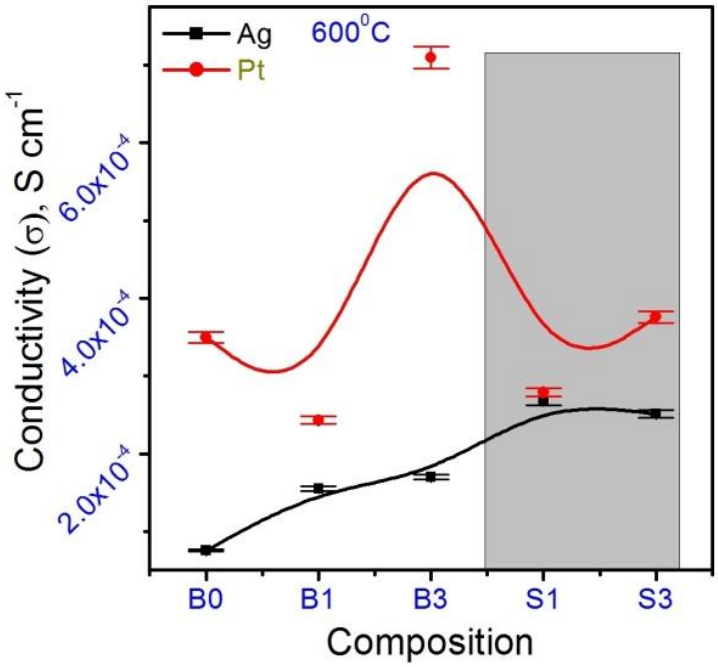

Figure 6.3: Values of dc conductivity obtained from the fitting of ac conductivity data using J P law

Fig. 6.3 shows the comparative plot of dc conductivity values extracted from the Jonscher Power Law fitting of ac conductivity data of the studied samples for Pt/M/Pt cell and Ag/M/Ag cell. At 600 °C, for instance, the conductivity σ_{Pt} for Pt/M/Pt cell configuration was found to be higher than conductivity σ_{Ag} of Ag/M/Ag cell configuration for all the compositions. However, the compositional variation is not same for two-cell configuration typically because of the values of B0 and B3. For B3, the value of conductivity σ_{Pt} for Pt/M/Pt cell configuration was increased by ≈1 order of magnitude than the conductivity σ_{Ag} for Ag/M/Ag cell configuration. Further, in order to study the electroding effect on ion dynamics, out of the various scaling mechanisms the conductivity spectra was scaled using hopping frequency (ν_h) as a scaling parameter known as Ghosh scaling [63]. Fig. 6.4 (a-d) shows the variation of $\log(\sigma/\sigma_{dc})$ vs $\log(\nu/\nu_o)$ for B0 and B3 specimens for the both cell configuration. It was observed that for B0 specimen, scaling was not achieved for Ag/B0/Ag and Ag/B3/Ag cell configuration at

higher temperatures whereas scaling was achieved at low temperature. However, for Pt/B0/Pt and Pt/B3/Pt cell configuration scaling was achieved at all.

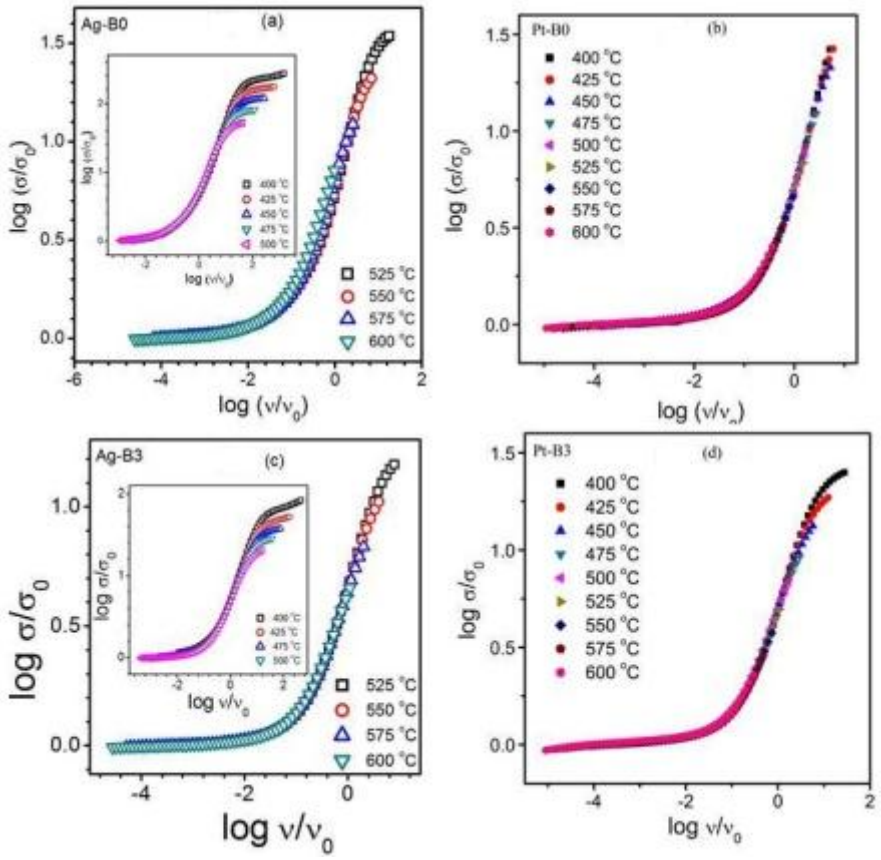

Figure 6.4: Variation of log σ/σ0 vs log ν/ν0 for B0 and B3

Fig. 6.5 (a-d) shows the variation of $\log(\sigma/\sigma_{dc})$ vs $\log(\nu/\nu_o)$ for both the cell configuration for S3 specimen. It was observed that for the both cell Ag/S3/Ag or Pt/S3/Pt scaling was not achieved overall range of the temperature.

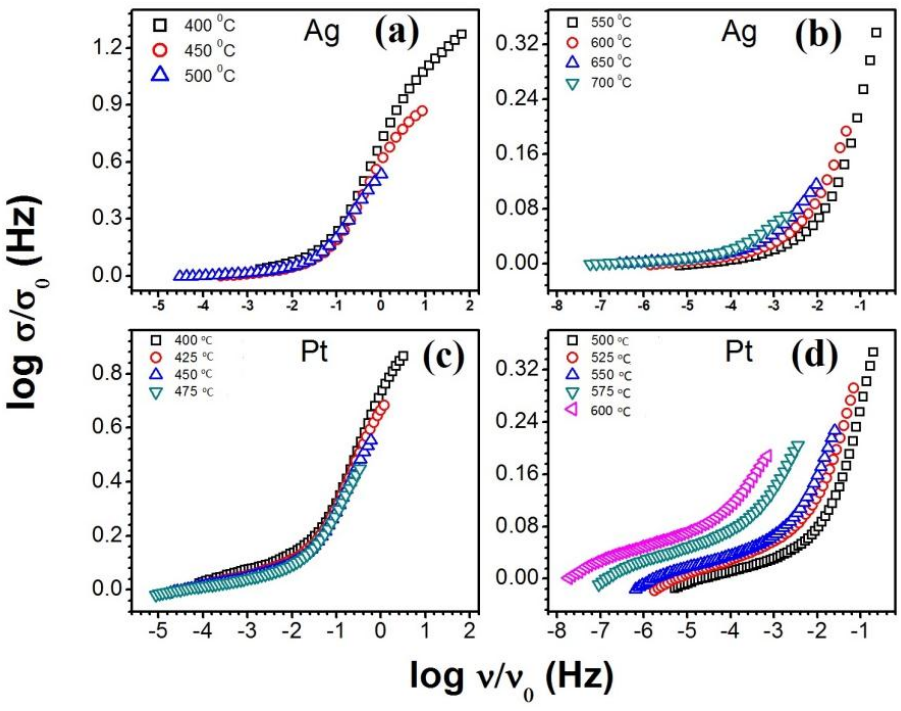

Figure 6.5: Variation of log σ/σ_0 vs log ν/ν_0 for S3

In order to understand such behaviour of scaling further, we have studied the exponent (n) for both of the cell configuration for all compositions and plotted them in Fig. 6.6 (a-c) as a function of temperature. In Ag/M/Ag, the value of the exponent (n) was smaller than its Pt counterpart. In cell configuration Ag/B0/Ag, the value of the exponent (n) was decreasing with increasing temperature, showing the large polaron hopping mechanism whereas, in Pt/B0/Pt, a change in slope of exponent value was observed where, firstly the exponent shows a minima at 450 ^{o}C with the increase in temperature followed by an increase in the temperature reveals the conversion of the large polaron to the small polaron hopping mechanism at 500 ^{o}C [68]. In Ag/B3/Ag configuration, the value of the exponent was increased to increase in temperature, showing the small polaron tunnelling mechanism. In Pt/B3/Pt cell configuration, a change in exponent (n)

behaviour was observed at ~500 ^{o}C, where, exponent is observed to be independent with temperature followed by an increase in exponent with temperature showing the conversion from correlated barrier hopping of polarons to small polaron tunnelling mechanism [68]. In both, Ag/S3/Ag and Pt/S3/Pt configuration, this change in slope was observed at 500 ^{o}C showing the conversion from small polaron hopping to large polaron hopping mechanism.

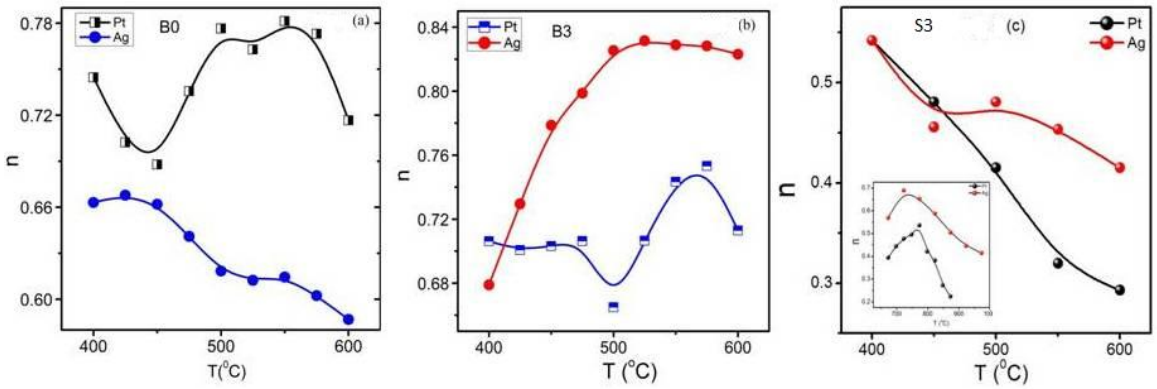

Figure 6.6: Variation of Exponent (n) with temperature for Ag/M/Ag and Pt/M/Pt cell configurations

6.3.4 Differential Impedance Analysis

The study of ion dynamics reveals different variation in the relaxation mechanism with frequency and temperature for Pt/M/Pt and Ag/M/Ag configuration. For relaxation mechanism, i.e. distribution of charge carriers around electrode/electrolyte different studies were adopted like, diffusion through the electrode/electrolyte interface, oxygen adsorption and dissociation on the electrode/electrolyte, bulk diffusion and triple phase boundary (TPB) diffusion, the charge transfer step involving formation of the oxygen anion around TPB and oxygen incorporation into the vacancy in the electrolyte, impedance formalism [106].

In order to verify the relaxation mechanism, we adopted impedance analysis technique and plotted the Impedance profile (Nyquist plot) at 600 ^{o}C for the both Pt/M/Pt and Ag/M/Ag configuration as shown in Fig. 6.7 and Fig. 6.7 (inset), respectively. In Pt/M/Pt configuration, it shows one resistance and one circular arc in the mid-frequency region and one spike in the high frequency region. Moreover, in Ag/M/Ag samples, nearly similar behavior with a small spike was observed instead of a large spike. Also, in Ag/M/Ag configuration high resistance was observed in comparison to Pt/M/Pt configuration. In order to correlate the electrical properties of the samples with the microstructure of the material, an equivalent circuit consisting of one resistance and one parallel R-Q circuit connected in series was used to interpret the nature of impedance plots using Z- view software (Fig. 6.7 inset). Here R and Q are the resistance and constant phase element for the semi-circular contributions. This indicates non-ideal behaviour of capacitance and occurrence of more than one relaxation processes with similar relaxation time.

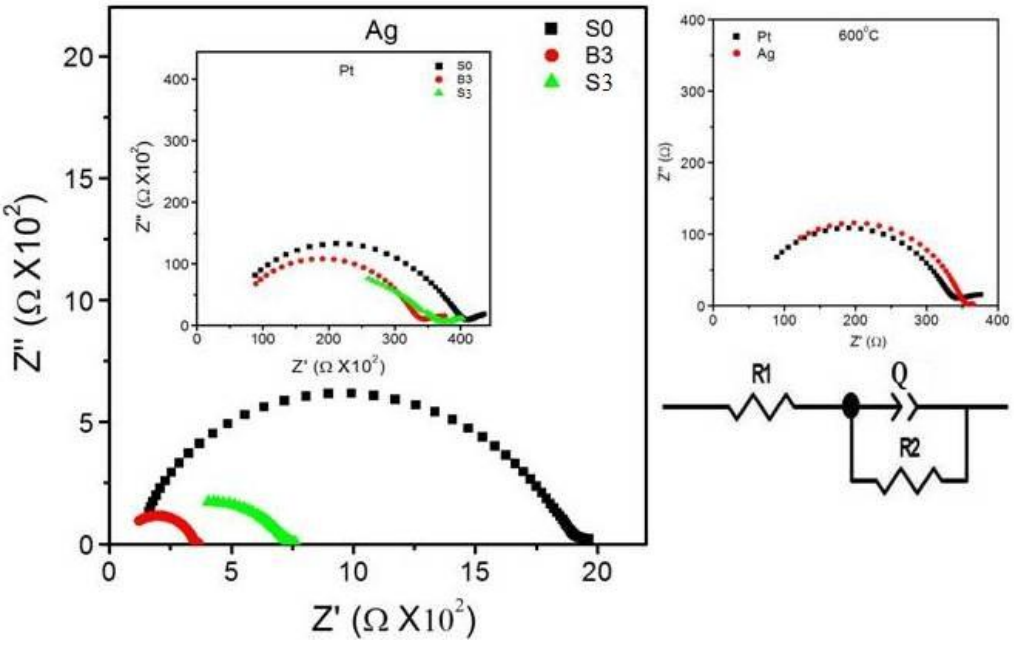

Figure 6.7: (a) Impedance profile (Nyquist plot) at 600 ^{o}C for Ag/M/Ag and Inset shows Nyquist plot for Pt/M/Pt **(b)** Nyquist plot for Ag/M/Ag and Pt/M/Pt showing the difference in electrode contributions **(c)** Equivalent circuit for the Nyquist plots

The capacitance of CPE is given by the relation $C = Q^K R^{(1-K)/K}$, where the parameter K knows as fractal exponent estimates the deviation from ideal capacitive behaviour [107]. The values of K are zero for the pure resistive case and unity for the pure capacitive one. The values of K were calculated from the slope of the corrected modulus, log|Z| vs log frequency plots in Fig. 6.8 (a-f). At high frequency, the corrected modulus is dominated by the contribution of the imaginary part of the impedance. The corrected modulus approaches zero, according to $|Z|_{adj} \approx f^{-K}$. Thus, the slope on a logarithmic plot has a value of –K at high frequencies. The values of K are plotted with the temperature for both the Ag/M/Ag and Pt/M/Pt configuration in Fig. 6.9 (a–c). Again, a change in behavior of K values for both of the cell configuration has been observed at ~500 ºC Usually, the value of K determines the roughness of the surface but the surface roughness gives the minute change. But in the present case, change in K values with the temperature, which can be attributed to the formation of ionic charge carriers in comparison to the deformation in the lattice [107].

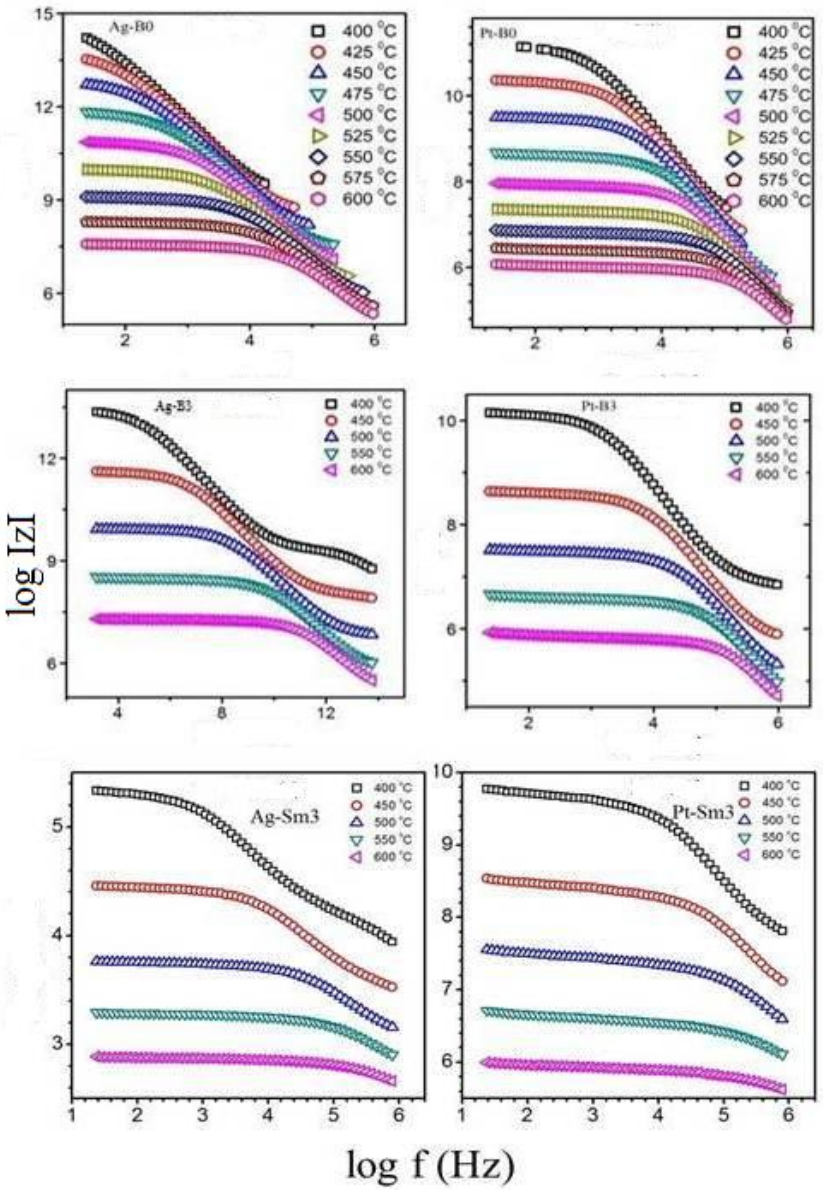

Figure 6.8: log |Z |vs log frequency plots to calculate the values of K

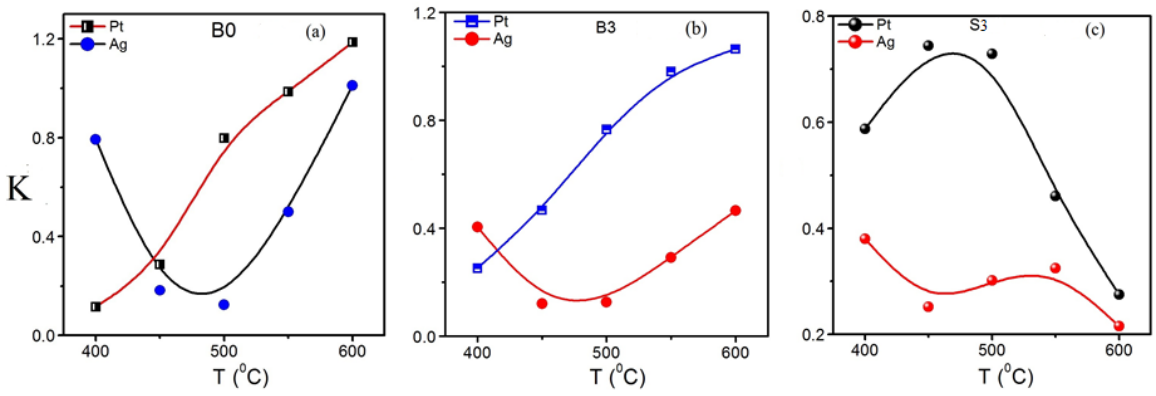

Figure 6. 9: Variation of the K values with temperature

The activation energy was calculated from the dc conductivity obtained from Jonscher power law fitting. Fig. 6.10 shows the ratio of $(E_a)_{Ag}$ for Ag/M/Ag cell configuration of activation energy $(E_a)_{Pt}$ Pt/M/Pt cell configuration for all the samples. Fig. 10 inset shows the variation of $\log(\sigma_{dc}\ T)$ vs 1000/T for the same. The activation energy obtained in Pt/M/Pt configuration was less than that of Ag/M/Ag cell configuration. Also, It was in good agreement with the activation energy obtained from the total conductivity using Nyquist plots (not shown here).

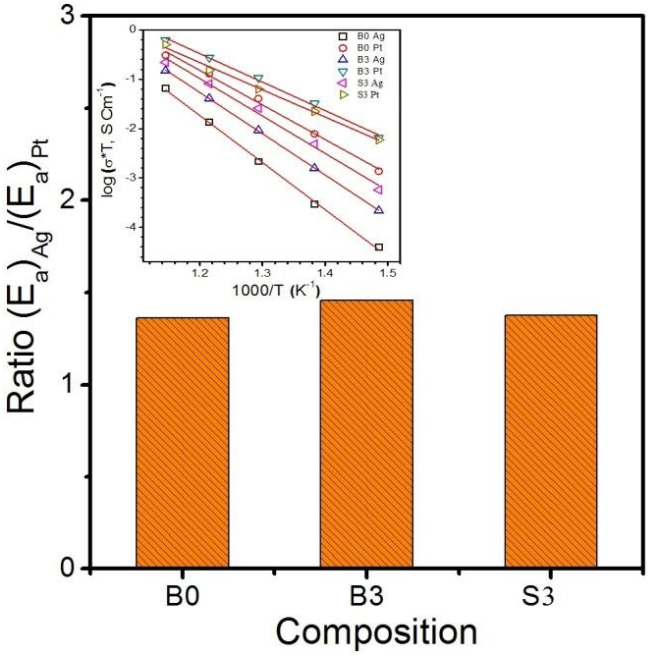

Figure 6.10: Ratio of Activation energy for Ag/M/Ag and Pt/M/Pt. The variation of log σT vs 1000/T (inset)

6.4 Microstructural Study of Ag and Pt at Interface

In the results section, it was observed that in Ag/B0/Ag and Ag/B3/Ag specimens Ghosh scaling was achieved at low temperature and low frequencies, whereas in Pt/B0/Pt and Pt/B3/Pt Ghosh scaling was achieved over all the range of temperature. But in Ag/S3/Ag and Pt/S3/Pt configuration, Ghosh scaling was not achieved at all. From exponent (n) behaviour, we have seen that for Ag/M/Ag, the value of the exponent (n)

was smaller in comparison to Pt/M/Pt. Further, we have observed that there is a change in hopping polaron length around 500 ^{o}C for each cell configuration. Here, it is necessary to mention that this is a zone boundary transition (ZBT), which is a characteristic feature of $LaAlO_3$. It is reported that at high temperatures, there is a phase transition from cubic to distorted rhombohedral phase. It is also pointed that it is associated to the atomic displacements explained by the transformations caused due to R25 or Γ25 phonon mode instability. In the present case, this transition or changing behaviour is more prominent with Pt electrode as Pt is felicitating the change in hopping polaron length from large polaron to small polaron or vice versa in comparison to Ag electrode. We are summarizing the results obtained from exponent behaviour in the following Table 6.1.

Table 6.1: Polaronic behavior of the investigate system before and after ZBT

Table 6.1		
Sample Name	**Before ZBT (Pt/M/Pt)/(Ag/M/Ag)**	**After ZBT (Pt/M/Pt)(Ag/M/Ag)**
B0	Large/Small	Small/Large
B3	CBH/Small	Small/CBH
S3	Small/Small	Large/Large

Now the question arises, why hopping polaron length is altered in Ag/M/Ag and Pt/M/Pt configurations. It was observed that in the Nyquist plots, there is a decrease in the value of resistance in Pt/M/Pt in comparison to Ag/M/Ag. To find reason for the decrease in resistance, CPE is analysed in the variation of fractal exponent (K). The similar variation was observed in the exponent behaviour (n) and was confirmed through fractal exponent (K) behaviour as measured through impedance bode plots. In Pt/B0/Pt configuration, there was a continuous increase in the value of K with temperature, whereas in Ag/B0/Ag configuration, a transition was observed. In both Pt/B3/Pt and

Ag/B3/Ag, similar behaviour was observed. This can be explained on the basis of the gradient of oxygen vacancies formed in the B0 and B3 specimens. The values of K are large in B0 and B3 samples in comparison to S3 sample for both of the cell configuration, but not a very large difference as seen in Fig.6.9. The small changes in the value of K from B0 to S3 can be correlated to the oxygen vacancy compensation as illustrated in the following equation using Kroger-vink notation as:

$$Sm_2O_3 + 0.1SrO + 0.1MgO + xAl_2O_3 \xrightarrow{(0.1+2x)LaAlO_3} 0.1Sr'_{La} + 0.1Mg'_{Al} + 2xSm_{La} + 2xAl^{\times}_{Al} + 0.2O_O + 0.1\,V^{\bullet\bullet}_O$$

Therefore, ionic conductivity of S3 should be smaller as compared to B0 and B3. To further verify the type of conductivity whether it is ionic or electronic, transport number using $T_f = 1-(\sigma_0/\sigma_g)$ has been evaluated (where, σ_0 is obtained from power law fitting curves and σ_g is obtained using low frequency semicircle in Nyquist plots) at different temperatures for Ag/M/Ag and Pt/M/Pt configuration [107]. Fig. 6.11 shows the transport number for the Ag/M/Ag and Pt/M/Pt specimens. In Ag/M/Ag and Pt/M/Pt specimens, transport number is greater than 0.85 showing that all samples are Type-I conductor. Further, Pt/M/Pt cell configuration has a transference number than that of Ag/M/Ag cell configuration. This reveals that Pt-electrode shows the better Electroding effect than that of Ag-electrode for ionic conduction relatively at high temperature. Also, there was change in slope observed at ~500 ^{o}C which is in good agreement with other observations observed in exponent and fractal exponent graphs.

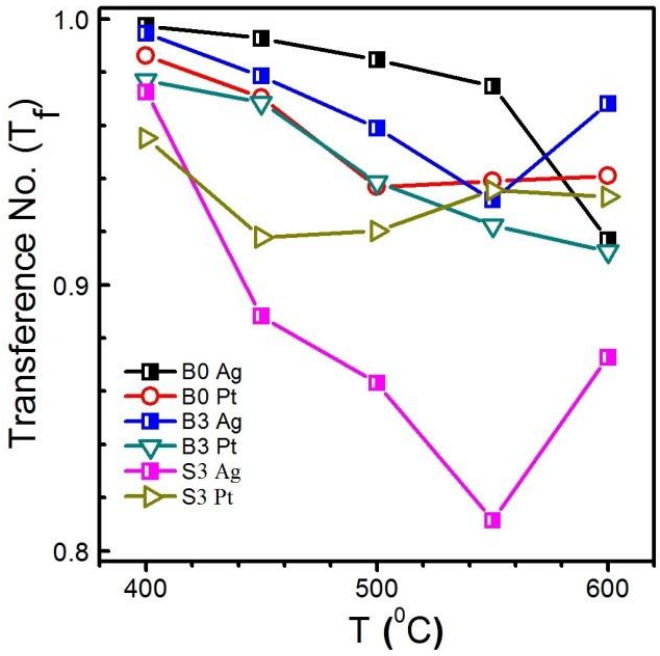

Figure 6.11: Transport number for Ag/M/Ag and Pt/M/Pt specimens

According to the transference number, at high temperature, B0 is highly ionic with high ionic conductivity in spite of the fact that B3 has higher value of conductivity. Now the cathodic process with the Pt and Ag electrodes needs to be inspected. For this, we have taken the microstructural study along with EDAX measurements.

6.5 Oxygen Ions Path at Interface: a proposed mechanism

In order to understand structural part and the electroding effect of Ag and Pt at the electrode-electrolyte interface, the SEM micrographs of Ag and Pt coated cross-section were taken and represented in Fig. 6.12 (a-e).

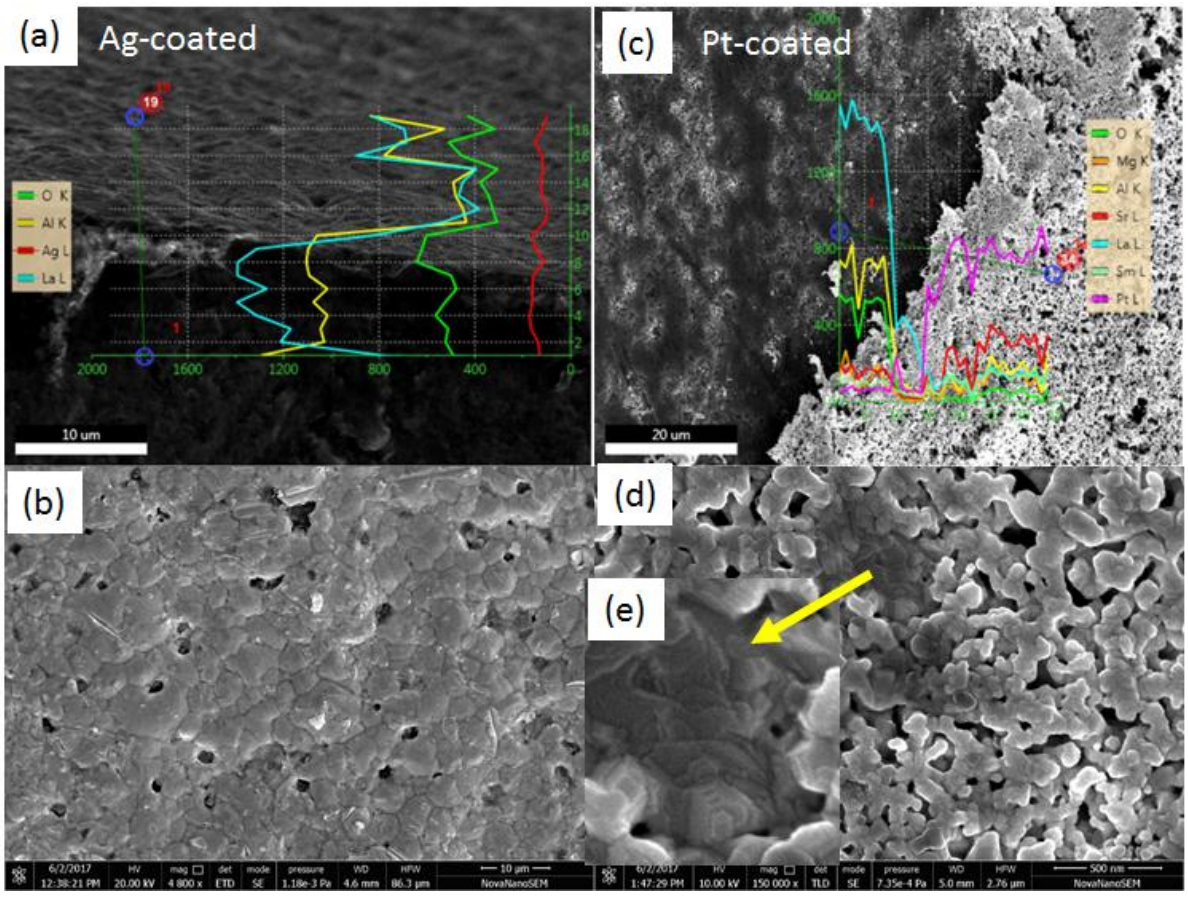

Figure 6.12: EDAX line profile for Ag/M/Ag and Pt/M/Pt specimen

The EDAX- line profile in Fig. 6.12 (a) clearly depicts that the line profile of Ag is approximately constant all over the cross-section of electrode-electrolyte interface has diffused into the electrolyte interface as shown through red line and O atom also shows nearly similar behaviour throughout the electrode-electrolyte interface as shown by the green line. The EDAX line profile in Fig. 6.12 (b) depicts that Pt line profile, i.e. intensity is not constant throughout the electrode-electrolyte interface as shown by magenta line and O line profile, i.e. intensity is also not constant all over the electrode-electrolyte interface region shown by the green line. This shows Ag has highly oxygen affinity property than that of Pt. From the SEM micrographs of the Pt and Ag cross-section, it is clear that Ag-electrode has dense grain structure (Fig. 6.12 (c)) and Pt-electrode has porous grain structure (Fig. 6.12 (d)). Also, it is well known that electrodes should be

porous structure for SOFC which is satisfied by Pt-electrode. The water-mark and lamellar features are observed in the Pt coating cross-section highlighted in Fig. 6.12 (e).

For the past decades, various conduction theories have been proposed for the electrode-electrolyte interface. The reaction is proposed as the reaction rate limiting one: gas diffusion or pore diffusion, gas diffusion layer diffusion, oxygen adsorption on Pt, dissociation of the oxygen molecule, surface diffusion of adsorbed oxygen on Pt, the charge transfer step, electronic conductivity, bulk diffusion of oxygen through Pt or electrolyte and vacancy diffusion. This rate-limiting step was quantitatively analysed in terms of resistance obtained through bound constant phase element behaviour. It can be analysed in terms of the value of the fractal exponent (K) i.e. K = 0.5 corresponds to diffusion limited transport in a bounded layer. The decrease in the value of the exponent with temperature informs for some changes in the transport of the species [94]. For $K \leq 0.35$, it describes the conductivity with the hindrances of the host matrix and the increase in the value of K from 0.5 to 0.8, which suggests increased surface accumulation of the oxygen species. In our work, the mechanism for our samples is illustrated in Table 6.2 and Fig. 6.13.

Table 6.2: Oxygen ions path for different electrode/electrolyte interface

Table 6.2

	B0		**B3**		**S3**	
	Before ZBT	After ZBT	Before ZBT	After ZBT	Before ZBT	After ZBT
Pt/M/Pt	$O_{2,surf}$	$O_{2,surf}$	$O_{2,surf}$	$O_{2,surf}$	$O_{2,surf}$	$trans_{species}$
Ag/M/g	Hi_{host}	$O_{2,surf}$	Hi_{host}	Hi_{host}	Hi_{host}	Hi_{host}

$trans_{species}$: transport of species, $O_{2,surf}$: Surface accumulation of O_2 species, Hi_{host}: Conductivity due to hindrance of the host ions

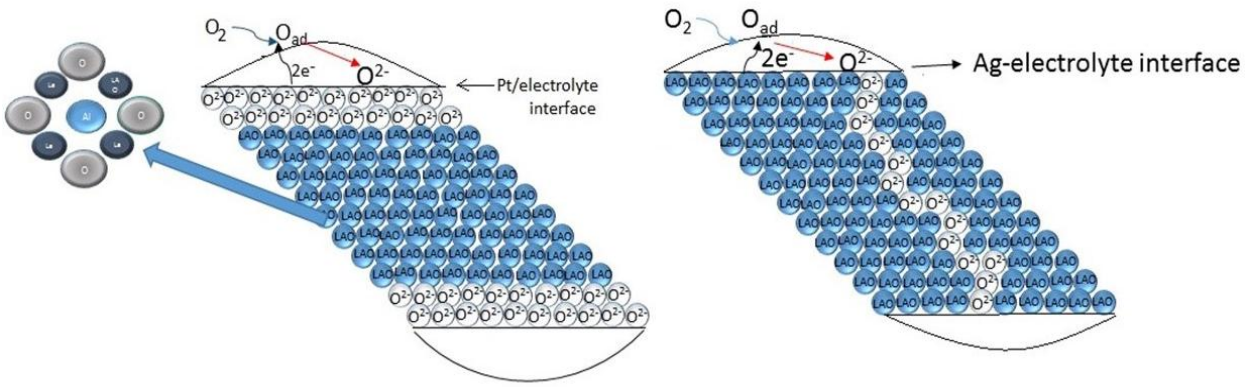

Figure 6.13: Pictorial representation for the motion of oxygen ions from the **(a)** Pt/M/Pt and **(b)** Ag/M/Ag

Fig. 6.13 gives the pictorial representation of the motion of oxygen ions from the electrode-electrolyte interface and through the electrolyte. The strong resistance changes near the electrode-electrolyte interface are explained with the strong electron lattice coupling and electric field induced structural changes. In our system, zone boundary transition around which there is a transition from small to large polaron or vice versa is related to the change in resistance mechanism from trapping to scattering. This change is assisting more in Pt/M/Pt rather than in Ag/M/Ag. However, the complete mechanism of formation of oxygen vacancies in Ag or Pt might be more complex, the continuous oxide ion channels have been altered in Ag and these channels are supported through Pt electrodes. The polaron hopping transition is more prominent in Pt/M/Pt in comparison to Ag/M/Ag due to the different propagation mechanisms of oxygen ions as illustrated in Fig. 6.13. However, for the more illustration of the mechanism, an oxygen reduction reaction mechanism needs to be studied through various oxygen partial pressures.

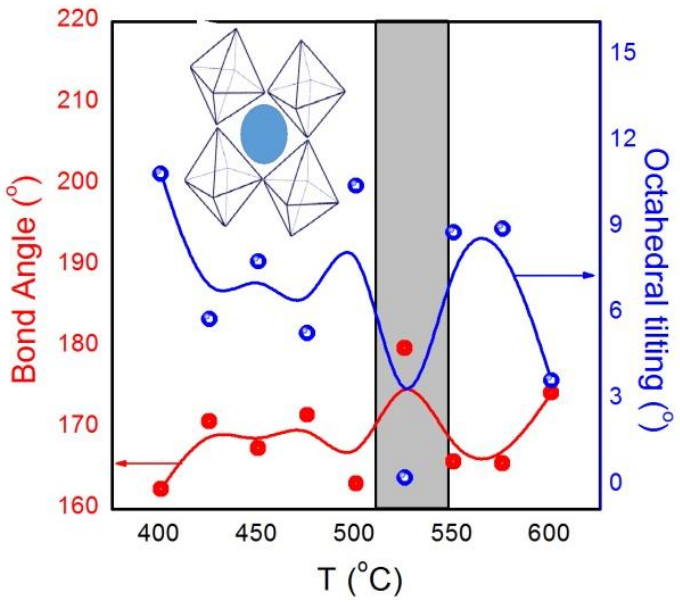

Figure 6.14: Bond angle and octahedral-tilting angle as a function of temperature

To correlate the zone boundary transition and polaron hopping, octahederal tilting has been studied. As octahedral tilting may be caused due to the coupling of band bending and strong local electric fields to the propagation of structural distortions created by oxygen vacancies [108]. To calculate the octahedral tilting at high temperature, HT-XRD measurements have been done. Through HT-XRD measurements, bond angle has been calculated using Diamond software after doing the reitveld refinements using R-3c symmetry of HT-XRD data (graphs not shown here). From this bond angle, the octahedral tilting angle has been calculated using relation

$$\cos^2\phi = \frac{2-2\cos\theta}{\cos\theta+5} \qquad 6.1$$

where, θ is the bond angle and ϕ is octahedral tilting.

Fig. 6.14 shows the bond angle and octahedral-tilting angle as a function of temperature. Inset shows the pictorial representation of octahedral tilting. It is observed

that the octahedral tilting is also showing a dip at ~500 ^{o}C confirming the zone boundary transition and the polaron hopping transition.

6.6 Conclusion

In order to study the electroding effect on oxide ion conduction, differential impedance analysis has been done on Ag/M/Ag and Pt/M/Pt cell configuration, where M = $(La_{0.9-x}(A)_x)Sr_{0.1}Al_{0.9}Mg_{0.1}O_{3-\delta}$ (A = Ba, Sm) for x = 0.00 and 0.03. All the studied samples shows type I ionic conductor with a transference number (T_f) is greater than and equal to 0.85. Also, high transference number (T_f) values for configuration Pt/M/Pt over Ag/M/Ag shows Pt as a better electrode for SOFC. Conductivity shows high values for Pt/M/Pt configuration than that of Ag/M/Ag configuration over all temperature range 400-600 ºC. In our system, zone boundary transition around which there is a transition from small to large polaron or vice versa is felicitated through Pt electrodes. It can be concluded that the Pt paste supports the motion of oxygen ions by not disturbing the inherent oxide ion channels of the electrolyte material, whereas Ag doesn't support the oxide ion channels as the value of fractal exponent indicates the hindrance created by the host ions.